

NLTE abundances of Eu for a sample of metal-poor stars in the Galactic Halo and Metal-poor Disk with 1D and <3D> models

Yanjun Guo^{1,2,3}, Nicholas Storm^{2,4}, Maria Bergemann², Jianhui Lian^{2,5}, Sofya Alexeeva⁶, Hongliang Yan^{6,9},
Yangyang Li⁷, Rana Ezzeddine^{7,8}, Gerber Jeffrey², and XueFei Chen¹

¹ Yunnan observatories, Chinese Academy of Sciences, P.O. Box 110, Kunming, 650011, China; guoyanjun@ynao.ac.cn

² Max-Planck Institute for Astronomy, Königstuhl 17, D-69117 Heidelberg, Germany

³ International Centre of Supernovae, Yunnan Key Laboratory, Kunming 650216, China

⁴ Heidelberg University, Grabengasse 1, 69117 Heidelberg, Germany;

⁵ South-Western Institute for Astronomy Research, Yunnan University, Kunming, Yunnan 650091, People's Republic of China

⁶ CAS Key Laboratory of Optical Astronomy, National Astronomical Observatories, Chinese Academy of Sciences, Beijing, 100101, People's Republic of China

⁷ Department of Astronomy, University of Florida, Bryant Space Science Center, Gainesville, FL 32611, USA

⁸ Joint Institute for Nuclear Astrophysics - Center for Evolution of the Elements, USA

⁹ Institute for Frontiers in Astronomy and Astrophysics, Beijing Normal University, Beijing 102206, China

December 10, 2024

ABSTRACT

Context. As a key to chemical evolutionary studies, the distribution of elements in galactic provides a wealth of information to understand the individual star formation histories of galaxies. The r-process is a complex nucleosynthesis process, and the origin of r-process elements is heavily debated. Europium (Eu) is viewed as an almost pure r-process element. Accurate measurements of europium abundances in cool stars are essential for an enhanced understanding of the r-process mechanisms.

Aims. We measure the abundance of Eu in solar spectra and a sample of metal-poor stars in the Galactic halo and metal-poor disk, with the metallicities ranging from -2.4 to -0.5 dex, using non-local thermodynamic equilibrium (NLTE) line formation. We compare these measurements with Galactic Chemical Evolution (GCE) models to explore the impact of the NLTE corrections on the contribution of r-process site in Galactic chemical evolution.

Methods. In this work, we use NLTE line formation, as well as one-dimensional (1D) hydrostatic and spatial averages of 3D hydrodynamical (<3D>) model atmospheres to measure the abundance of Eu based on both the Eu II 4129 Å and Eu II 6645 Å lines for solar spectra and metal-poor stars.

Results. We find that for Eu II 4129 Å line the NLTE modelling leads to higher (0.04 dex) solar Eu abundance in 1D and higher (0.07 dex) in <3D> NLTE while NLTE modelling leads to higher (0.01 dex) solar Eu abundance in 1D and lower (0.03 dex) in <3D> NLTE for Eu II 6645 Å line. Although the NLTE corrections for the Eu II λ 4129 Å and Eu II λ 6645 Å lines are opposite, the discrepancy between the abundances derived from these individual lines reduces after applying NLTE corrections, highlighting the critical role of NLTE abundance determinations. By comparing these measurements with Galactic chemical evolution (GCE) models, we find that the amount of NLTE correction does not require significant change of the parameters for Eu production in the GCE models.

Key words. Galaxy: evolution Catalogs; Sun: abundances – Chemical abundances; Stellar evolution;

1. Introduction

Abundance ratios as a function of time or metallicity provide important information about the scenarios of nucleosynthesis and also allow us to trace the chronology of events in Galaxy, since different chemical elements are produced on different time scales in different astrophysical sites (Rana 1991; Wilson & Rood 1994; Chiappini et al. 2003; Matteucci 2012, 2014). Iron peak elements such as iron, cobalt, and chromium, are produced over longer time-scales in Type Ia supernovae (Burbidge et al. 1957; Nomoto et al. 1994; Hillebrandt & Niemeyer 2000; Seitzzahl et al. 2013; Bergemann et al. 2019a). In addition, the abundance of α -elements such as magnesium and oxygen has been demonstrated to be a sensitive proxy for the initial phases of Galactic chemical evolution, which are dominated by the production of heavy elements and the return from core-collapse supernovae (Tinsley 1980; Woosley & Heger 2015). Slow neutron-

capture process (s-process) elements, like strontium and barium, are produced in intermediate and low-mass asymptotic giant branch (AGB) stars (Tinsley 1980; Pagel 1997; Matteucci 2001; Karakas & Lattanzio 2014; Frischknecht et al. 2016; Choplin et al. 2018). Similar, rapid neutron-capture process (r-process) elements, such as europium, provide insight into violent events such as neutron star mergers, neutron-driven winds in core-collapse SNe, explosions of rapidly rotating magnetised massive stars (Rosswog et al. 1999; Takahashi et al. 1994; Woosley et al. 1994; Arcones & Thielemann 2013; Bliss et al. 2018; Siegel et al. 2019; Reichert et al. 2023).

While numerous studies have provided detailed insights into the chemical evolution of α -elements and iron peak elements, there is a paucity of theoretical and observational data available for neutron capture elements, especially for the r-process elements (Woosley & Heger 2015; Frischknecht et al. 2016;

Choplin et al. 2018; Lian et al. 2023). The r-process is a complex process that requires extremely high neutron density, making the origin of r-process elements remains a topic of ongoing debate in the scientific community (Burbidge et al. 1957; Martin et al. 2015; Siegel & Metzger 2017; Côté et al. 2018a; Halevi & Mösta 2018; Radice et al. 2018; Siegel et al. 2019). Europium is almost a pure r-process element (Snedden et al. 2008; Cowan et al. 2021). Thus, precise measurements of Eu abundances in cool stars are crucial for constraining the sites of nucleosynthetic production.

Guiglian et al. (2018) investigated three pure r-process elements, including Eu, Gd, and Dy based on MARCS model atmosphere and the local thermodynamic equilibrium (LTE) code. They found that the [Eu/Fe] ratio follows a continuous sequence from the thin disk to the thick disk with respect to metallicity. Lian et al. (2023) compared the evolution of the [Eu/Fe]-[Fe/H] trend, based on Eu abundance measurements using 1D LTE model, with the GCE model in the metal-rich region. However, their study lacks a metal-poor sample and relies solely on 1D LTE results. As shown in recent literature studies (Bergemann & Nordlander 2014a,b; Bergemann et al. 2017a; Storm & Bergemann 2023; Storm et al. 2024), it is crucial to take into account the effects of NLTE and 3D effects for FGKM-type stars. Therefore, further study of applying NLTE and <3D> corrections to Eu abundances in a metal-poor sample is essential.

The first analysis of NLTE effects in Eu can be traced back to Mashonkina & Gehren (2000), which presents the statistical equilibrium of Eu II using a model atom that includes 32 levels of Eu II along with the ground state of Eu III and derives the solar europium abundance with $A(\text{Eu}) = 0.53$ dex. Zhao et al. (2016) follow the atomic model from Mashonkina & Gehren (2000) and investigate Eu abundances in 1D NLTE analysis. Recently, Storm et al. (2024) published the latest Eu atom model with 163 levels of Eu II to investigate the solar abundance of Eu. In this work, we apply NLTE line formation, as well as 1D hydrostatic and <3D> model atmospheres with the latest Eu atomic data from Storm et al. (2024) to measure the abundance of Eu of 164 metal-poor stars in the Galactic halo and metal-poor disk with [Fe/H] ranging from -2.4 to -0.5 dex adopted from Ruchti et al. (2011).

The structure of the paper is as follows. We introduce our observed data in Section. 2. In Section 3, we describe the detail of method we use to analysis the abundance of Eu. The best-fit results for the Sun and the comparison with GCE model are presented in Sec. 4. Finally, we summarize our conclusions in Sec. 6.

2. Data

The sample is adopted from Ruchti et al. (2011). It includes 319 metal-poor stars in Galactic disk and halo with the effective temperature (T_{eff}) ranging from 4050 to 6500 K, the surface gravity ($\log g$) ranging from 0.5 to 4.5, the metallicities ranging from -2.8 to -0.5 dex. These stars were selected to investigate thick disk-like kinematics, and were originally observed by the RAVE survey (Steinmetz et al. 2006). The sample was observed using several high-resolution facilities, include the MIKE spectrograph on the Magellan-Clay telescope (Bernstein et al. 2003), FEROS on the MPG 2.2 m telescope (Kaufer et al. 1999), the UCLES spectrograph on the Anglo-Australian telescope (Walker & Diego 1985), and the ARC spectrograph on the Apache Point 3.5 m telescope (Wang et al. 2003). The wavelength range of the spectra observed from UCLES is from 4460 to 7270 Å, while the other three cover the full optical range from 3500 to ~ 9500

Å. The signal-to-noise ratios (S/N) of all the spectra are greater than 100 pixel^{-1} at around 6000 Å. We adopted the NLTE-opt stellar parameters from Table 1 in Bergemann et al. (2017b) as the input data for our further analysis.

3. Methods

Here, we will provide a description of the model atmospheres, spectral synthesis code, NLTE models, and linelist that we use in this work.

3.1. Model Atmospheres

We used two grids of models to analyze our metal-poor sample: the 1D line-blanketed hydrostatic MARCS model from Gustafsson et al. (2008) and the average 3D model (hereafter, <3D>) Stagger model from Magic et al. (2013a,b).

The MARCS model is a homogeneous model atmosphere for late-type (FGKM) stars, assuming LTE. This model uses the thermal equilibrium and Saha equation for all number densities of atoms and molecules (Gibson & Heitler 1928; Russell 1934), as well as the Boltzmann distribution for all partition functions and excitation equilibrium (Irwin 1981; Gustafsson et al. 2008). The MARCS model atmospheres provided ≈ 16000 standard composition model atmospheres¹ covering a wide parameter space: The range of effective temperature (T_{eff}) are from 2500K to 8000K, with a step of 100K for (T_{eff}) from 2500K to 4000K and a step of 250K for all other ones. For surface gravity ($\log g$), the range is from -1 to 5.0 dex with a step of 0.5 dex. The range of metallicity ([Fe/H]) is from -5.0 to 1.0, with a step of 0.25 dex from -1.0 to 1.0 dex, 0.5 dex from -3.0 to 1.0, and 1 dex from -5.0 to -3.0 . The micro-turbulence, with four different values of 0, 1, 2 and 5 km s^{-1} , is also included in the grids.

The grid of Stagger model atmospheres is a collection of three-dimensional (3D) and time-dependent hydrodynamic model atmospheres with a more realistic treatment of the radiative transfer equation for late-type stars (Magic et al. 2013a,b). The grid of <3D> Stagger model atmospheres used in this work is an average of such sets of Stagger model atmospheres on surfaces of equal optical depth ($\log \tau_{5000}$) also adopted from (Magic et al. 2013a,b). The grid models presented by Magic et al. (2013a) consist of approximately 220 models, which can be found on their website². The models cover the following ranges of stellar parameters: effective temperature (T_{eff}) from 4000 K to 7000 K with a step size of 500 K, surface gravity ($\log g$) from 1.5 to 5.0 dex with a step size of 0.5 dex, and metallicity ([Fe/H]) from -4.0 to 0.5 dex with a step size of 0.5 dex from -1 to 0.5 dex, and 1.0 dex from -4.0 to -1 dex.

3.2. Spectral synthesis code

Turbospectrum (TS) is a spectral synthesis code based on LTE radiative transfer (Feautrier 1964; Nordlund 1984; Alvarez & Plez 1998; Plez 2012). The TS code has been continuously developed over the years, and recently the latest version v20.0³ was published. The most significant update in this version is the ability to generate NLTE spectra. Similar to other abundance analysis and spectrum synthesis codes, this is achieved by using grids of NLTE departure coefficients to calculate the NLTE line pro-

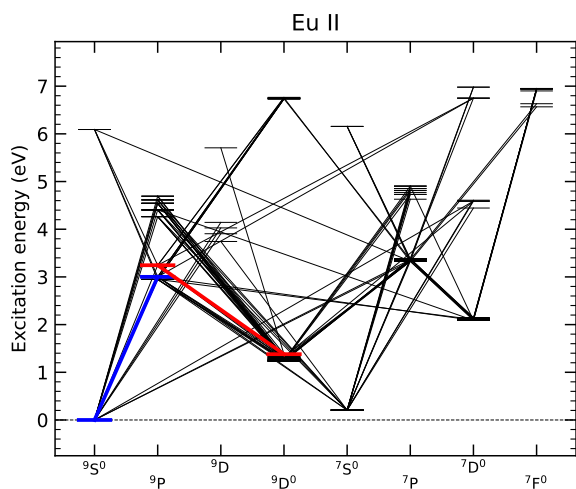
¹ <https://marcs.astro.uu.se>

² <https://staggergrid.wordpress.com>

³ <https://github.com/bertrandplez/Turbospectrum2020>

Table 1. The Eu II line used for abundance calculations.

λ Å	Lower level	Upper level	$\log gf$
4129.7	$a^9S_0^0$	z^9P_4	0.22
6645.1	$a^9D_6^0$	z^9P_5	0.12

**Fig. 1.** Grotrian diagram of the Eu II model atom. The model atom are taken from the Storm et al. (2024). The blue and red lines represent the transitions giving rise to the Eu II 4129 Å and 6645 Å lines, respectively.

files by correcting the line source functions and the line opacity of all lines (further details described in Gerber et al. 2023).

A Python wrapper called Turbospectrum Spectral Fitting with Python (TSFitPy)⁴ developed by Gerber et al. (2023) is specifically designed to determine stellar abundances, optional with other parameters such as micro-turbulence (ξ_t) using the Nelder-Mead (simplex algorithm) minimization method (Nelder & Mead 1965; Wright 1996). TSPfitPy was notably updated to fit either macroturbulence or rotation for each individual line using L-BFGS-B (Limited-memory Broyden-Fletcher-Goldfarb-Shanno with bound consideration) algorithm (Byrd et al. 1995; Zhu et al. 1997) using the Scipy Python package (Virtanen et al. 2020). This is done as a secondary step after generating synthetic spectra with a specific stellar abundance to break the degeneracy of fitting the abundance and the broadening of lines simultaneously (Storm & Bergemann 2023). A dedicated interpolating function is provided together with TS code, which takes the rectangular grids of model atmospheres and the corresponding grids of departure coefficients, and produces an interpolated atmosphere structure and departure file for a desired combination of stellar parameters (Gerber et al. 2023).

In this work, we use the updated TSPfitPy and TS code to fit observed spectra and obtain the stellar abundances of the metal-poor sample.

3.3. NLTE models

We adopted the NLTE model of Eu from Storm et al. (2024), which utilizes data from the NIST⁵ and Kurucz⁶ databases (Mar-

tin et al. 1978; Nakhate et al. 2000; Johnson & Nelson 2017). The electronic structure of Eu comprises a total of 662 levels, with Eu I having 498 levels and Eu II having 163 levels. The ionization potentials for Eu I and Eu II are 5.67 eV and 11.24 eV, respectively (Martin et al. 1978). The atom model of Eu contains three ionisation stages and is closed by the Eu III state. The Grotrian diagram of the Eu II model atom is shown in Fig. 1.

We use MULTI1D code to compute statistical equilibrium (SE) calculations, which was developed by Carlsson (1986). MULTI1D code solves the SE equations iteratively and handles the radiative transfer equation in a 1D plane-parallel geometry, assuming that deviations from LTE do not influence the structure of the input model atmosphere, which underlies the standard assumption of a trace element to calculate the statistical equilibrium of NLTE elements. Recently, the MULTI1D was updated by our group (Bergemann et al. 2019a; Gallagher et al. 2020) and are widely used for NLTE analyses of atmospheric parameters and chemical abundances (Gerber et al. 2023; Storm & Bergemann 2023; Li & Ezzeddine 2023).

We use a Python wrapper⁷ for MULTI1D to calculate the departure coefficients of Eu for both grids of MARCS and <3D> Stagger model atmospheres (using the same methodology as in Sec. 2.4 in Gerber et al. 2023). For each individual star, we obtain the abundance directly using TS by fitting the spectra, where the NLTE synthetic spectra are based on the precomputed departure coefficients from MULTI1D. As detailed, the europium departure coefficient grids are computed between [Eu/Fe] = -2 to +1 in steps of 0.1 dex. During the fitting process, the closest departure coefficient within [Eu/Fe] step is used (within 0.05 dex) for the synthetic spectra generation. For example a star with [Eu/Fe] = 0.6 dex would use departure coefficients computed with that specific abundance. Therefore, different [Eu/Fe] abundances are taken into account during the statistical equilibrium calculations for each individual star.

3.4. Linelist and line choice

We use the homogeneous Gaia-ESO linelist, which contains atomic and molecular data from Heiter et al. (2021) and was recently updated by Magg et al. (2022) with atomic data for several elements. For the solar Eu abundance, we adopt $A(\text{Eu}) = 0.57$ from Storm et al. (2024). For Eu II lines, the gf -values were measured by Lawler et al. (2001) based on experimental life-times and branching fractions (BFs).

Eu II 4129.73 Å is the resonance line most widely used in Eu abundance determinations (Mashonkina & Gehren 2000; François et al. 2007; Zhao et al. 2016; Lucchesi et al. 2024). Eu II 6645.10 Å is the strongest Eu II line in the yellow-red spectral region and is partially blended with weak Si I lines at 6645.21 Å in the solar spectrum (Lawler et al. 2001). It is also reliably used in stellar Eu abundance studies (Mashonkina & Gehren 2000; Lawler et al. 2001; Heiter et al. 2021; Storm et al. 2024). Therefore, the final abundance analysis primarily relies on these two Eu II line feature. The atomic parameters of these two lines are provided in Table. 1.

There are two odd isotopes for Eu which are ¹⁵¹Eu and ¹⁵³Eu. The solar isotopic abundance ratio for this two isotopes is set to 47.8:52.2, respectively from Lodders et al. (2009). The Eu II 4129 Å line is represented by 11 individual hyperfine splitting (HFS) components from Mashonkina & Gehren (2000). The Eu

⁷ https://github.com/stormnick/wrapper_multi

⁴ <https://github.com/JGerbs13/TSFitPy>

⁵ https://physics.nist.gov/PhysRefData/ASD/levels_form.html

⁶ <http://kurucz.harvard.edu/atoms/6301/>

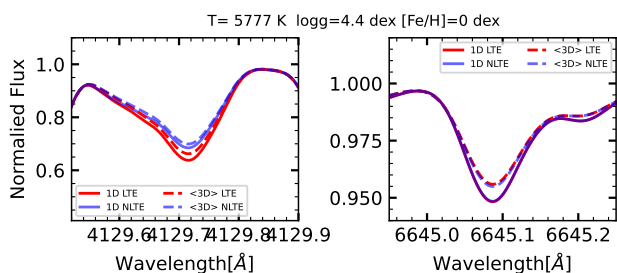


Fig. 2. The synthetic spectra for Eu II 4129Å (left) and Eu II 6645Å (right) generated from TSPyFit base on solar parameter with $A(\text{Eu})=0.57$ dex. The red solid lines represent the line profile generated from 1D LTE and the blue solid lines are from 1D NLTE, while the red dash lines represent the line profile generated from <3D> LTE and the blue dash lines are from <3D> NLTE.

II 6645Å line is represented by 11 hyperfine and isotopic components (Storm et al. 2024).

4. Results

4.1. Synthetic spectra

To showcase TSPyFit capability, we generated the spectra with 1D LTE/NLTE and <3D> LTE/NLTE lines profiles based on solar parameters for Eu II 4129Å (left) and Eu II 6645Å (right) in Figure 2. The red solid lines represent line profiles generated from 1D LTE, while the blue solid lines are from 1D NLTE. The red dashed lines represent line profiles generated from <3D> LTE, and the blue dashed lines are from <3D> NLTE. From the comparison of the red and blue lines in the left panel, we observe that the NLTE effect weakens the Eu II 4129Å line in both 1D and <3D> models. By comparing the red and blue solid lines in the right panel, we find that the NLTE effect slightly weakens the line in the 1D model. This result is consistent with the positive 1D NLTE correction found by Mashonkina & Gehren (2000) and Storm et al. (2024). In contrast, when comparing the red and blue dashed lines, we observe that the NLTE effect strengthens the line in the <3D> model. Storm et al. (2024) studied the impact of full 3D NLTE modeling of Eu on solar abundances. They found that the Eu NLTE model results in a slightly positive correction in 1D and a negative correction in 3D, which is consistent with our findings.

4.2. Solar Eu abundance

In the top panels of Fig. 3, we show the observed Sun spectrum of the selected Eu II λ 4129Å line (left) and Eu II λ 6645Å (right) line in black dots, taken from the Vacuum Vertical Telescope at the Institute für Astrophysik Göttingen (IAG) with the resolving power of $R = 700,000$ (Reiners et al. 2016). We overplot the synthetic spectrum based on the 1D NLTE model with the best-fit $A(\text{Eu}) = 0.61 \pm 0.05$ for λ 4129Å line and $A(\text{Eu}) = 0.55 \pm 0.05$ for λ 6645Å line in red lines, and the synthetic spectrum based on the <3D> NLTE model with the best-fit $A(\text{Eu}) = 0.64 \pm 0.05$ for λ 4129Å line and $A(\text{Eu}) = 0.58 \pm 0.05$ for λ 6645Å line in blue lines. We accounted for the blending of the Eu II λ 4129.7 Å line by Ti I λ 4129.66 Å line and Sc I λ 4129.75 Å (Mashonkina & Gehren 2000). For Eu II λ 6645.70 Å line, we accounted for the blending of Si I λ 6645.21 line. For different stars in Sec. 4.4, the Ti, Sc and Si abundance was scaled to [Fe/H]. The individual error components were calculated by adding the systematic uncertainty (including blends and uncertainty of f -values) and the

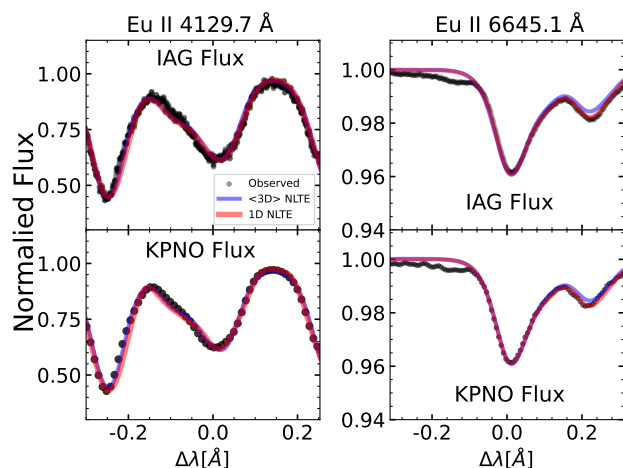


Fig. 3. The best fitting synthetic spectra of sun for λ 4129Å (left panels) and Eu II λ 6645Å (right panels) generated from TSPyFit. The red line and blue line represent the synthetic spectra based on 1D and <3D> NLTE, respectively. The observed data are shown as black dots.

fitting error in quadrature (Storm et al. 2024). In the bottom panels of Fig. 3, we present the observed Sun spectrum in black dots, derived from the solar Kitt Peak National Observatory (KPNO) FTS atlas with $R \approx 400,000$ (Kurucz et al. 1984). The synthetic spectrum based on the 1D NLTE model with the best-fit $A(\text{Eu}) = 0.62 \pm 0.05$ for λ 4129Å line and $A(\text{Eu}) = 0.58 \pm 0.05$ for λ 6645Å line are overplotted in red, and the synthetic spectrum based on the <3D> NLTE model with the best-fit $A(\text{Eu}) = 0.64 \pm 0.05$ for λ 4129Å line and $A(\text{Eu}) = 0.60 \pm 0.05$ for λ 6645Å line are shown in blue. This indicates that the Eu abundances derived from the 1D NLTE model are consistent across the two observed spectra, and similarly, the results from the <3D> NLTE model are also consistent. The best-fit values of 1D LTE and <3D> LTE, are also provided in Table. 2.

Our results for 1D LTE and NLTE abundances are higher than those reported by Mashonkina & Gehren (2000), who obtained LTE and NLTE abundances for λ 4129Å line are 0.49 and 0.53 and for λ 6645Å line are 0.50 and 0.53, respectively. The differences could be attributed to several factors, including the different $\log g_f$ values used in our study (0.22 for λ 4129Å line and 0.12 for λ 6645Å line from Lawler et al. (2001); see Section 3.3), compared to the value of 0.174 for λ 4129Å and 0.204 for λ 6645Å taken from Komarovskii (1991) in Mashonkina & Gehren (2000). Additionally, the Eu II lines are also influenced by hyperfine structure and isotopic shifts. We used hyperfine structure data described in Section 3.4 for the Eu II λ 6645Å line, represented with 11 hyperfine and isotopic components from Storm et al. (2024), whereas Mashonkina & Gehren (2000) used data from Biehl (1976). The Eu isotope ratio used in Mashonkina & Gehren (2000) was 55:45, whereas we used a ratio of 47.8:52.2 from Lodders et al. (2009) based on the Gaia-ESO line list (Heiter et al. 2021). Furthermore, we used the MULTI1D code to calculate the statistical equilibrium of Eu, while Mashonkina & Gehren (2000) used the NONLTE3 code. Besides, due to these differences in atomic data and the statistical equilibrium code, Storm et al. (2024) tested the main factors influencing the results and concluded that they are primarily due to the use of a more comprehensive atomic model.

Our 1D LTE/NLTE Eu abundances obtained from Eu II λ 6645Å line (0.57 ± 0.05 and 0.58 ± 0.05) are in good agreement with Storm et al. (2024), who reported values of $0.59 \pm 0.01_{\text{stat}} \pm$

Table 2. Derived A(Eu) abundances based on 1D and <3D> LTE/NLTE models for IAG and KPNO spectra.

Spectra	1D LTE	1D NLTE	<3D> LTE	<3D> NLTE
IAG flux (4129)	0.54	0.61	0.59	0.64
KPNO flux (4129)	0.55	0.62	0.59	0.64
IAG flux (6645)	0.54	0.55	0.60	0.58
KPNO flux (6645)	0.57	0.58	0.63	0.60

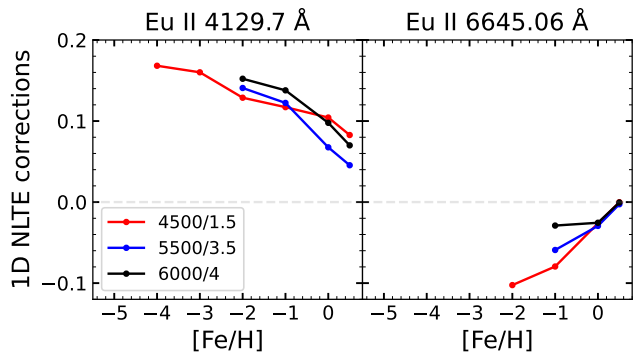


Fig. 4. The NLTE corrections for Eu II λ 4129 Å line (left panel) and λ 6645 Å line (right panel) are plotted against the metallicity [Fe/H] of the model atmospheres. The red line represents the NLTE correction of red giant with parameters of $T_{\text{eff}}=4500$ K/ $\log g=1.5$ dex, the blue line represents the NLTE correction of subgiant with parameters of $T_{\text{eff}}=5500$ K/ $\log g=3.5$ dex and the black line represents the NLTE correction of main-sequence star with parameters of $T_{\text{eff}}=6000$ K/ $\log g=4.0$ dex. The NLTE calculations were performed assuming [Eu/Fe] = 0.

0.06_{sys} and 0.60 ± 0.01_{stat} ± 0.06_{sys}. The 1D LTE/NLTE Eu abundances of IAG spectrum are slightly lower than their results, but still within their error bar. Although the log g values and the 1D model atmosphere used are the same, these differences could still arise from different radiative transfer codes, calculations of departure coefficients, as they use the MULTI3D@DISPATCH code (Eitner et al. 2024), while we use Turbospectrum and MULTI1D for NLTE calculations (see Sect. 3.3). The obtained discrepancies between these two codes are within 0.05 dex for the strong lines, e.g. Mn lines (Storm et al. in prep). Similarly, Bergemann et al. (2012) and Bergemann et al. (2019b) used the same model atom and got slightly different results using different codes.

The difference for Eu II λ 6645 Å line in abundance corrections is consistent with findings from Storm et al. (2024), showing an increasing between 1D LTE and 1D NLTE, and a decreasing from <3D> (full 3D) LTE to <3D> (full 3D) NLTE. However, our <3D> results are higher than their full 3D results, which are 0.58 and 0.55. This may indicate that <3D> cannot represent all of the 3D effects, but nevertheless provides a great insight into its effects.

4.3. NLTE effects on Eu II lines

Fig. 4 shows the NLTE corrections for Eu II λ 4129 Å line (left panel) and λ 6645 Å lines (right panel) plotted against the metallicity [Fe/H] of the model atmospheres. The red line depicts the NLTE correction for red giants (RG) with parameters of $T_{\text{eff}}=4500$ K/ $\log g=1.5$, while the black line illustrates the NLTE correction for main-sequence stars (MS) with parameters of $T_{\text{eff}}=6000$ K/ $\log g=4.0$. Additionally, the blue line represents the NLTE correction of subgiant (SG) with parameters of $T_{\text{eff}}=5500$ K/ $\log g=3.5$. The NLTE corrections for Eu II λ 4129 Å are

positive, while negative or close to zero for Eu II λ 6645 Å. For Eu II λ 4129 Å line, at values of [Fe/H] near -2 dex, the corrections for RG, SG, and MS are close to each other. For Eu II λ 6645 Å line, the NLTE corrections for RG are slightly higher than those for SG, and the corrections for SG are slightly higher than those for MS stars when [Fe/H] is less than 0 dex. For the MS, the NLTE corrections do not exceed -0.03 dex at [Fe/H] = -1 dex. However, for RG, the NLTE corrections can reach -0.1 dex at [Fe/H] = -2 dex. It also indicates that the NLTE corrections increase with decreasing metallicity, which may have an impact on the GCE trend of [Eu/Fe] especially with the lower [Fe/H] (Alexeeva et al. 2023; Storm et al. 2024). Although the NLTE corrections for the Eu II λ 4129 Å and Eu II λ 6645 Å lines are entirely opposite, the final results after NLTE corrections match (as discussed in Section 4.4), further proving the necessity of NLTE corrections for determination of Eu abundance.

We show the departure coefficients, b_i , for Eu II λ 6645 Å line as a function of optical depth in Fig. 5. Here, the departure coefficient $b_i = \frac{n_i^{\text{NLTE}}}{n_i^{\text{LTE}}}$ is defined as the ratio of the NLTE population of atomic level n_i^{NLTE} to the LTE population of atomic level n_i^{LTE} . The solid lines represent the lower levels, while the dashed lines represent the upper levels. The departure coefficients for the solar model atmosphere are depicted in red, while the black one represents the model atmosphere with $T_{\text{eff}} = 4500$ K, $\log g = 2.0$ dex, and [Fe/H] = -1 dex. We chose this model atmosphere because its parameters are similar to those of most of our sample stars. The formation height is shown as + at $\log(\tau) = 0$ for line center. In the solar atmosphere, the formation height of 6645 Å line corresponds to $\log(\tau_{500}) = -0.64$, where both states $z^9P_5^0$ and a^9D_6 tend to be overpopulated compared to LTE values, with b_j being higher than b_i at the same time. According to Bergemann & Nordlander (2014a), this suggests that the line source function exceeds the Planck function ($S_{\nu}^l/B_{\nu}^l \approx b_j/b_i > 1$). As a result, line became weaker under NLTE conditions relative to LTE. This ultimately causes slightly positive NLTE corrections. For the model atmosphere with $T_{\text{eff}} = 4500$ K, $\log g = 2.0$ dex, and [Fe/H] = -1 dex, another effect plays a more important role. The departure coefficient of upper energy state is closer to that of lower energy state ($b_i \approx b_j$) at $\log(\tau_{500}) = -0.6$. Thus, the enhanced line opacity compared to LTE (since $\kappa^l \approx b_i > 1$), increases the number of absorbed photons. This enhanced absorption strengthens the line under NLTE conditions, leading to a negative NLTE correction.

We present the fitting results of four stars as examples in Fig. 6. For Eu II 4129 Å line, We present the observed spectrum as black dots in the upper left panel with parameters of $T_{\text{eff}}=4852$ K, $\log g=2.12$ dex, [Fe/H]=-1.65 dex and in the lower left panel with $T_{\text{eff}}=4988$ K, $\log g=2.53$ dex, [Fe/H]=-1.43 dex. For Eu II 6645 Å line, we show the observed spectrum in black dots with parameters of $T_{\text{eff}}=4995$ K, $\log g=2.42$ dex, [Fe/H]=-1.8 dex in the upper right panel and $T_{\text{eff}}=4401$ K, $\log g=1.13$ dex, [Fe/H]=-1.41 dex in the lower right panel. The red and blue lines represent the best-fit synthetic spectra based on 1D LTE and

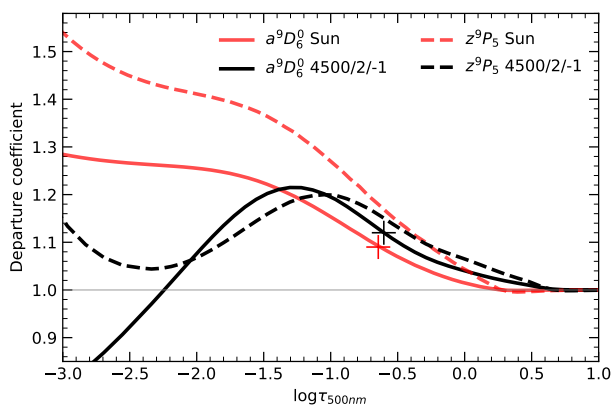


Fig. 5. Departure coefficients for Eu II λ 6645 Å line as a function of optical depth. The solar model atmosphere are depicted in red and $T_{\text{eff}}=4500$ K/ $\log g=2.0$ dex/ $[\text{Fe}/\text{H}]=-1$ dex in black, with solid and dashed lines representing lower and upper levels, respectively.

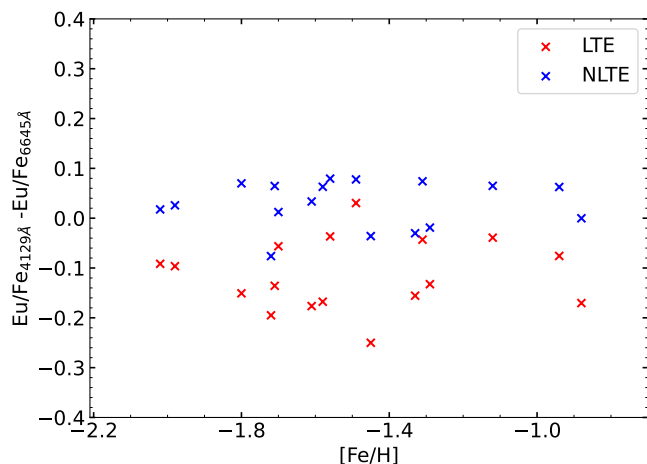


Fig. 7. Comparison of Eu/Fe differences between the λ 4129 Å and λ 6645 Å lines under LTE (black) and NLTE (red) conditions.

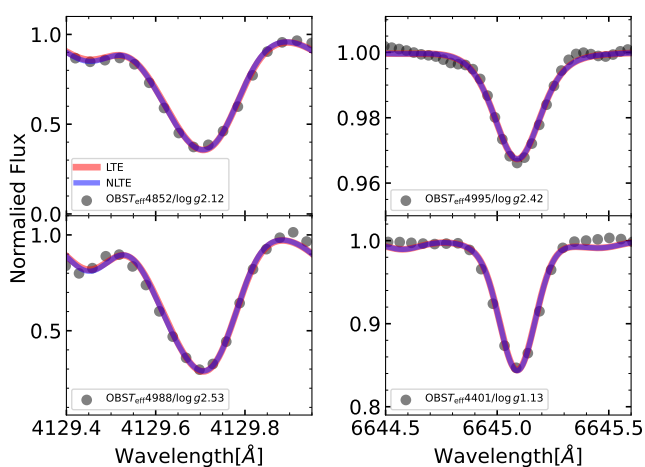


Fig. 6. The examples of the fitting based on 1D LTE (red line) and NLTE (blue line) model. The black dots in each panel represent the observed spectrum with four different stars.

NLTE models, respectively. We show the comparison of Eu/Fe differences between the λ 4129 Å and λ 6645 Å lines in Fig. 7. The NLTE corrections result in more consistent values between the two lines, highlighting the importance of NLTE corrections for precise Eu abundance determinations.

4.4. Comparison of the results with GCE model

The wavelength range for some of our stars does not include the Eu II 4129 Å line, and in some cases, both the Eu II 4129 Å and Eu II 6645 Å lines are blended or very weak. Therefore, the results presented below are only for the spectra that were well fitted with a total of 164 stars having metallicities ranging from -2.4 to -0.5 dex. However, the $\langle 3D \rangle$ grid covers a smaller range of atmospheric parameters (Magic et al. 2013a,b) and thus only a small part of our sample of stars was fitted with these models. Therefore, our results are only based on the results of the 1D. All the best fitting results are provide in Tab. 3 for Eu II 4129 Å and Tab. 4 for Eu II 6645 Å. There are five stars in our sample that are carbon-enhanced metal-poor with s-process element enhancement (CEMP-s) stars (Placco et al. 2018), which

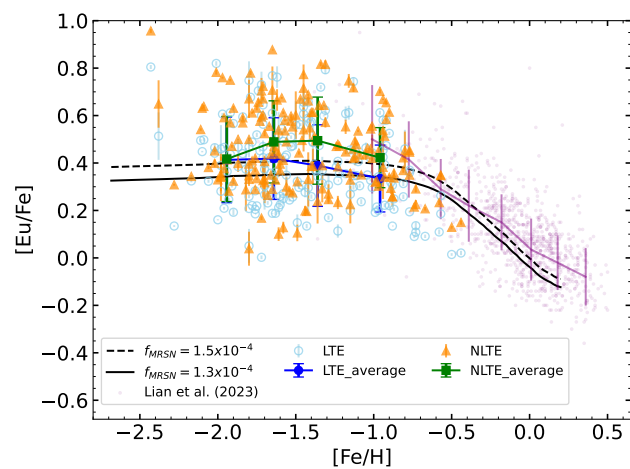


Fig. 8. The trend of $[\text{Eu}/\text{Fe}]$ based on the best fitting results of 1D NLTE and LTE. The green squares and blue dots represent the averaged NLTE and LTE $[\text{Eu}/\text{Fe}]$ ratios across the selected bins. The yellow triangles and cyan circles represent the NLTE and LTE $[\text{Eu}/\text{Fe}]$ for each stars. The purple dots represent 1D LTE Eu abundance measurements of 1274 metal-rich stars from Gaia-ESO survey. The dashed and solid lines represent the GCE models with different fraction of massive stars that end up with MRSN instead of CCSN.

do not follow the Galactic chemical evolution trend, and we use * to mask them in Table 3 and 4.

Fig. 8 shows the $[\text{Eu}/\text{Fe}]$ based on 1D NLTE of our metal-poor sample as a function of $[\text{Fe}/\text{H}]$ combined with 1D LTE Eu abundance measurements of 1274 metal-rich stars from Gaia-ESO survey (Gilmore et al. 2022; Randich et al. 2022) with high spectral signal-to-noise ratio ($\text{SNR} > 50$; Lian et al. 2023). We divided the bins to ensure approximately an equal number of stars in each, with the green squares and blue dots representing the averaged NLTE and LTE $[\text{Eu}/\text{Fe}]$ ratios across the selected bins. The yellow triangles and cyan circles represent the NLTE and LTE $[\text{Eu}/\text{Fe}]$ values for a total of 141 stars based on the λ 4129 Å line and 35 stars based on the λ 6645 Å line combined. As shown in Fig. 8, the trend of $[\text{Eu}/\text{Fe}]$ is almost flat in metal-poor region and both the scatter of data points and the NLTE adjustments tend to decrease from low to high metallicity. However, this phenomenon requires confirmation with more data points in the future.

Table 3. Results of Eu Abundance based on Eu II 4129 Å line.

Spectra	T_{eff}	$\log g$	[Fe/H]	ξ_t	[Eu/Fe] _{IDLTE}	[Eu/Fe] _{IDNLTE}
RAVE J004733.4-450942	4925	2.18	-1.78	1.5	0.42	0.56
RAVE J022308.0-312953	4783	1.93	-1.65	1.9	0.56	0.68
RAVE J022658.3-074959	5125	2.84	-1.71	1.2	0.43	0.57
RAVE J031005.5-401003	5065	2.68	-1.35	1.5	0.46	0.58
RAVE J031535.8-094744	4774	2.06	-1.31	1.6	0.58	0.65

This table is available in its entirety in machine-readable form. The first five entries are shown here for guidance regarding its format and content.

Table 4. Results of Eu Abundance based on Eu II 6645 Å line.

Spectra	T_{eff}	$\log g$	[Fe/H]	ξ_t	[Eu/Fe] _{IDLTE}	[Eu/Fe] _{IDNLTE}
TYC 8789-00425-1	4383	1.22	-1.56	2.1	0.35	0.30
TYC 9161-00706-1	4992	2.02	-1.39	1.6	0.49	0.39
RAVE J212558.5-265657	4795	2.04	-1.61	1.9	0.52	0.44
RAVE J204547.1-621403	4995	2.42	-1.8	1.5	0.75	0.67
RAVE J104943.6-092646	4695	2.04	-1.13	1.6	0.74	0.72

This table is available in its entirety in machine-readable form. The first five entries are shown here for guidance regarding its format and content.

For comparison, the tracks of two galactic chemical evolution (GCE) models generated by OMEGA+ Côté et al. (2018b) using the parameters of the basic model in Lian et al. (2023) are presented. In these models, to account for the rapid decrease of [Eu/Fe] in metal-rich regime which implies much shorter release timescale of Eu than Fe by SN-Ia, the contribution of Eu in short timescale from magneto rotating supernova (MRSN) has been taken into account in addition to the neutron star merger (NSM) which releases Eu in much longer timescales (Côté et al. 2019). For NSM we assume an ejecta mass of $2.5 \times 10^{-2} M_{\odot}$ with yields table from Arnould et al. (2007) and occurrence rate of 2×10^{-5} for every solar mass of star formation. The delay time distribution of NSM is assumed to follow a power law in the form of t^{-1} with minimum delay time of 10 Myr and maximum delay time of 10^6 Gyr. To include the contribution of MRSN, we replace a tiny fraction (0.013% and 0.015%) of core-collapse supernova (CCSN) in the mass range of 13-25 M_{\odot} by MRSN and use the yields table from Nishimura et al. (2015). This fraction is higher than that (0.01%) adopted in Lian et al. (2023) in which the data in the low metallicity regime is limited and the fraction of MRSN is not well constrained. In this work we intend to test the impact of the NLTE corrections on the required parameters responsible for Eu production in GCE models. For simplicity, we focus on one of the key and poor constrained parameter, the fraction of MRSN in CCSN (f_{MRSN}), which is positively correlated with the [Eu/Fe] abundance in old metal-poor stars. As expected, with higher [Eu/Fe] after NLTE correction, a GCE model with larger f_{MRSN} is needed to well fit the average [Eu/Fe] of our sample. We note that the required change in (f_{MRSN}) is not substantial given the NLTE correction derived in this work.

5. Summary

Eu, as an r-process element, provides insight into violent events such as neutron star mergers, helping us to better understand nucleosynthetic production sites. Due to the lack of observational data for r-process elements, especially for Eu based on NLTE analysis in the metal-poor region, this work aims to improve the

understanding of Eu abundances in metal-poor stars by applying NLTE and <3D> corrections.

We performed a detailed analysis of the NLTE effects on Eu II 4129 Å and Eu II 6645 Å for a sample of metal-poor stars. For Eu II 4129 Å line, we found that the NLTE effects result in positive NLTE abundance correction in both 1D and <3D> in solar atmosphere. For Eu II 6645 Å line, we found that the NLTE effects result in a slightly positive NLTE abundance correction in 1D and a negative one in <3D> in solar atmosphere. Although the NLTE corrections for the Eu II λ 4129 Å and Eu II λ 6645 Å lines are entirely opposite, the discrepancy between the abundances derived from individual lines decreases after NLTE fitting, once again showcasing the importance of NLTE abundance determination. Finally, we show the trend of [Eu/Fe] as a function of [Fe/H] and compare it with the GCE models. It indicates that the NLTE correction does not require significant change of the parameter for the Eu production in GCE models. However, due to the limitations of observational data and models, this phenomenon requires confirmation with more data points, e.g. 4MOST in the future.

6. Data availability

Tables 3 and 4 are only available in electronic form at the CDS via anonymous ftp to cdsarc.u-strasbg.fr (130.79.128.5) or via <http://cdsweb.u-strasbg.fr/cgi-bin/qcat?J/A+A/>.

Acknowledgements. This work is supported by the Natural Science Foundation of China (Nos. 12288102, 12125303, 12090040/3, 12103064, 12403039, 12373036), the National Key R&D Program of China (grant Nos. 2021YFA1600403/1, 2021YFA1600400), and the Natural science Foundation of Yunnan Province (Nos. 202201BC070003, 202001AW070007), the International Centre of Supernovae, Yunnan Key Laboratory (No. 202302AN360001) and the “Yunnan Revitalization Talent Support Program”-Science and Technology Champion Project (NO. 202305AB350003). NS and MB acknowledge funding from the European Research Council (ERC) under the European Union’s Horizon 2020 research and innovation programme (Grant agreement No. 949173). MB is supported through the Lise Meitner grant from the Max Planck Society. H.-L.Y. acknowledges support from the Youth Innovation Promotion Asso-

ciation of the CAS. We acknowledge support by the Collaborative Research centre SFB 881 (projects A5, A10), Heidelberg University, of the Deutsche Forschungsgemeinschaft (DFG, German Research Foundation).

References

- Alexeeva, S., Wang, Y., Zhao, G., et al. 2023, *ApJ*, 957, 10
- Alvarez, R. & Plez, B. 1998, *A&A*, 330, 1109
- Arcones, A. & Thielemann, F. K. 2013, *Journal of Physics G Nuclear Physics*, 40, 013201
- Arnould, M., Goriely, S., & Takahashi, K. 2007, *Phys. Rep.*, 450, 97
- Bergemann, M., Collet, R., Amarsi, A. M., et al. 2017a, *ApJ*, 847, 15
- Bergemann, M., Collet, R., Schönrich, R., et al. 2017b, *ApJ*, 847, 16
- Bergemann, M., Gallagher, A. J., Eitner, P., et al. 2019a, *A&A*, 631, A80
- Bergemann, M., Gallagher, A. J., Eitner, P., et al. 2019b, *A&A*, 631, A80
- Bergemann, M., Lind, K., Collet, R., Magic, Z., & Asplund, M. 2012, *MNRAS*, 427, 27
- Bergemann, M. & Nordlander, T. 2014a, in *Determination of Atmospheric Parameters of B*, 169–185
- Bergemann, M. & Nordlander, T. 2014b, *arXiv e-prints*, arXiv:1403.3088
- Bernstein, R., Shectman, S. A., Gunnels, S. M., Mochnacki, S., & Athey, A. E. 2003, in *Society of Photo-Optical Instrumentation Engineers (SPIE) Conference Series*, Vol. 4841, *Instrument Design and Performance for Optical/Infrared Ground-based Telescopes*, ed. M. Iye & A. F. M. Moorwood, 1694–1704
- Biehl, D. 1976, PhD thesis, -
- Bliss, J., Arcones, A., & Qian, Y. Z. 2018, *ApJ*, 866, 105
- Burbidge, E. M., Burbidge, G. R., Fowler, W. A., & Hoyle, F. 1957, *Reviews of Modern Physics*, 29, 547
- Byrd, R. H., Lu, P., Nocedal, J., & Zhu, C. 1995, *SIAM Journal on Scientific Computing*, 16, 1190
- Carlsson, M. 1986, *Uppsala Astronomical Observatory Reports*, 33
- Chiappini, C., Romano, D., & Matteucci, F. 2003, *MNRAS*, 339, 63
- Choplin, A., Hirschi, R., Meynet, G., et al. 2018, *A&A*, 618, A133
- Côté, B., Denissenkov, P., Herwig, F., et al. 2018a, *ApJ*, 854, 105
- Côté, B., Eichler, M., Arcones, A., et al. 2019, *ApJ*, 875, 106
- Côté, B., Silvia, D. W., O’Shea, B. W., Smith, B., & Wise, J. H. 2018b, *ApJ*, 859, 67
- Cowan, J. J., Sneden, C., Lawler, J. E., et al. 2021, *Reviews of Modern Physics*, 93, 015002
- Eitner, P., Bergemann, M., Hoppe, R., et al. 2024, *A&A*, 688, A52
- Feautrier, P. 1964, *Comptes Rendus Academie des Sciences (serie non specifiée)*, 258, 3189
- François, P., Depagne, E., Hill, V., et al. 2007, *A&A*, 476, 935
- Frischknecht, U., Hirschi, R., Pignatari, M., et al. 2016, *MNRAS*, 456, 1803
- Gallagher, A. J., Bergemann, M., Collet, R., et al. 2020, *A&A*, 634, A55
- Gerber, J. M., Magg, E., Plez, B., et al. 2023, *A&A*, 669, A43
- Gibson, G. E. & Heitler, W. 1928, *Zeitschrift für Physik*, 49, 465
- Gilmore, G., Randich, S., Worley, C. C., et al. 2022, *A&A*, 666, A120
- Guiglian, G., de Laverny, P., Recio-Blanco, A., & Prantzos, N. 2018, *A&A*, 619, A143
- Gustafsson, B., Edvardsson, B., Eriksson, K., et al. 2008, *A&A*, 486, 951
- Halevi, G. & Mösta, P. 2018, *MNRAS*, 477, 2366
- Heiter, U., Lind, K., Bergemann, M., et al. 2021, *A&A*, 645, A106
- Hillebrandt, W. & Niemeyer, J. C. 2000, *ARA&A*, 38, 191
- Irwin, A. W. 1981, *ApJS*, 45, 621
- Johnson, D. A. & Nelson, P. G. 2017, *Journal of Physical and Chemical Reference Data*, 46, 013108
- Karakas, A. I. & Lattanzio, J. C. 2014, *PASA*, 31, e030
- Kaufer, A., Stahl, O., Tubbesing, S., et al. 1999, *The Messenger*, 95, 8
- Komarovskii, V. A. 1991, *Optics and Spectroscopy*, 71, 322
- Kurucz, R. L., Furenlid, I., Brault, J., & Testerman, L. 1984, *Solar flux atlas from 296 to 1300 nm*
- Lawler, J. E., Wickliffe, M. E., den Hartog, E. A., & Sneden, C. 2001, *ApJ*, 563, 1075
- Li, Y. & Ezzeddine, R. 2023, *AJ*, 165, 145
- Lian, J., Storm, N., Guiglian, G., et al. 2023, *MNRAS*, 525, 1329
- Lodders, K., Palme, H., & Gail, H. P. 2009, *Landolt Börstein*, 4B, 712
- Lucchesi, R., Jablonka, P., Skúladóttir, Á., et al. 2024, *A&A*, 686, A266
- Magg, E., Bergemann, M., Serenelli, A., et al. 2022, *A&A*, 661, A140
- Magic, Z., Collet, R., Asplund, M., et al. 2013a, *A&A*, 557, A26
- Magic, Z., Collet, R., Hayek, W., & Asplund, M. 2013b, *A&A*, 560, A8
- Martin, D., Perego, A., Arcones, A., et al. 2015, *ApJ*, 813, 2
- Martin, W. C., Zalubas, R., & Hagan, L. 1978, *Atomic energy levels - The rare-Earth elements*
- Mashonkina, L. & Gehren, T. 2000, *A&A*, 364, 249
- Matteucci, F. 2001, *The chemical evolution of the Galaxy*, Vol. 253
- Matteucci, F. 2012, *Chemical Evolution of Galaxies*
- Matteucci, F. 2014, in *Saas-Fee Advanced Course*, Vol. 37, *Saas-Fee Advanced Course*, ed. J. Bland-Hawthorn, K. Freeman, & F. Matteucci, 145
- Nakhate, S. G., Razvi, M. A. N., Connerade, J. P., & Ahmad, S. A. 2000, *Journal of Physics B Atomic Molecular Physics*, 33, 5191
- Nelder, J. A. & Mead, R. 1965, *The Computer Journal*, 7, 308
- Nishimura, N., Takiwaki, T., & Thielemann, F.-K. 2015, *ApJ*, 810, 109
- Nomoto, K., Yamaoka, H., Shigeoyama, T., Kumagai, S., & Tsujimoto, T. 1994, in *Supernovae*, ed. S. A. Bludman, R. Mochkovitch, & J. Zinn-Justin, 199
- Nordlund, A. 1984, in *Methods in Radiative Transfer*, 211–233
- Pagel, B. E. J. 1997, *Nucleosynthesis and Chemical Evolution of Galaxies*
- Placco, V. M., Beers, T. C., Santucci, R. M., et al. 2018, *AJ*, 155, 256
- Plez, B. 2012, *Turbospectrum: Code for spectral synthesis*, *Astrophysics Source Code Library*, record ascl:1205.004
- Radice, D., Perego, A., Hotokezaka, K., et al. 2018, *ApJ*, 869, 130
- Rana, N. C. 1991, *ARA&A*, 29, 129
- Randich, S., Gilmore, G., Magrini, L., et al. 2022, *A&A*, 666, A121
- Reichert, M., Obergaulinger, M., Aloy, M. Á., et al. 2023, *MNRAS*, 518, 1557
- Reiners, A., Mrotzek, N., Lemke, U., Hinrichs, J., & Reinsch, K. 2016, *A&A*, 587, A65
- Rosswog, S., Liebendörfer, M., Thielemann, F. K., et al. 1999, *A&A*, 341, 499
- Ruchtig, G. R., Fulbright, J. P., Wyse, R. F. G., et al. 2011, *ApJ*, 737, 9
- Russell, H. N. 1934, *ApJ*, 79, 317
- Seitenzahl, I. R., Cescutti, G., Röpke, F. K., Ruitter, A. J., & Pakmor, R. 2013, *A&A*, 559, L5
- Siegel, D. M., Barnes, J., & Metzger, B. D. 2019, *Nature*, 569, 241
- Siegel, D. M. & Metzger, B. D. 2017, *Phys. Rev. Lett.*, 119, 231102
- Snedden, C., Cowan, J. J., & Gallino, R. 2008, *ARA&A*, 46, 241
- Steinmetz, M., Zwitter, T., Siebert, A., et al. 2006, *AJ*, 132, 1645
- Storm, N., Barklem, P. S., Yakovleva, S. A., et al. 2024, *A&A*, 683, A200
- Storm, N. & Bergemann, M. 2023, *MNRAS*, 525, 3718
- Takahashi, K., Wittig, J., & Janka, H. T. 1994, *A&A*, 286, 857
- Tinsley, B. M. 1980, *Fund. Cosmic Phys.*, 5, 287
- Virtanen, P., Gommers, R., Oliphant, T. E., et al. 2020, *Nature Methods*, 17, 261
- Walker, D. D. & Diego, F. 1985, *MNRAS*, 217, 355
- Wang, S.-i., Hildebrandt, R. H., Hobbs, L. M., et al. 2003, in *Society of Photo-Optical Instrumentation Engineers (SPIE) Conference Series*, Vol. 4841, *Instrument Design and Performance for Optical/Infrared Ground-based Telescopes*, ed. M. Iye & A. F. M. Moorwood, 1145–1156
- Wilson, T. L. & Rood, R. 1994, *ARA&A*, 32, 191
- Woolley, S. E. & Heger, A. 2015, *ApJ*, 810, 34
- Woolley, S. E., Wilson, J. R., Mathews, G. J., Hoffman, R. D., & Meyer, B. S. 1994, *ApJ*, 433, 229
- Wright, M. 1996, *Direct search methods: Once scorned, now respectable*, ed. D. Griffiths & G. Watson (Addison-Wesley), 191–208
- Zhao, G., Mashonkina, L., Yan, H. L., et al. 2016, *ApJ*, 833, 225
- Zhu, C., Byrd, R. H., Lu, P., & Nocedal, J. 1997, *ACM Trans. Math. Softw.*, 23, 550–560